

Modeling Wall Film Formation and Breakup Using an Integrated Interface-Tracking/Discrete-Phase Approach

M. Arienti¹

e-mail: arientm@utrc.utc.com

L. Wang

M. Corn

X. Li

M. C. Soteriou

United Technologies Research Center,
411 Silver Lane,
East Hartford, CT 06108

T. A. Shedd

University of Wisconsin,
Madison, WI 53706

M. Herrmann

Arizona State University,
Tempe, AZ 85287

We propose a computationally tractable model for film formation and breakup based on data from experiments and direct numerical simulations. This work is a natural continuation of previous studies where primary atomization was modeled based on local flow information from a relatively low-resolution tracking of the liquid interface [Arienti and Soteriou, 2007, "Dynamics of Pulsed Jet in Crossflow," ASME Paper No. GT2007-27816]. The submodels for film formation proposed here are supported by direct numerical simulations obtained with the refined level set grid method [Herrmann, 2008, "A Balanced Force Refined Level Set Grid Method for Two-Phase Flows on Unstructured Flow Solver Grids," J. Comput. Phys., 227, pp. 2674–2706]. The overall approach is validated by a carefully designed experiment [Shedd et al., 2009, "Liquid Jet Breakup by an Impinging Air Jet," Forty-Seventh AIAA Aerospace Sciences Meeting, Paper No. AIAA-2009-0998], where the liquid jet is crossflow-atomized in a rectangular channel so that a film forms on the wall opposite to the injection orifice. The film eventually breaks up at the downstream exit of the channel. Comparisons with phase Doppler particle analyzer data and with nonintrusive film thickness point measurements complete this study. [DOI: 10.1115/1.4002019]

1 Introduction

The injection and atomization of liquid fuels is important to many combustion devices, including gas turbines and internal combustion engines. Fuel droplet size, fuel spray spatial distribution, and fuel/air mixing are all critical performance metrics for the injection systems that directly affect combustion performance.

One common method of fuel atomization involves creating a thin film of fuel along a solid surface, and then subjecting that film to shear from high-velocity air flows. This process occurs in various types of internal combustion engines in which fuel can impinge on the walls of the combustion chamber. Because of stringent emissions regulations, it is important to avoid the formation of unburned hydrocarbons, particularly in cold start conditions. For this reason, various researchers have studied film and droplet formation from the impingement of a spray onto a film in the absence of a crossflow of air [1], as well as in the presence of crossflow [2,3].

Of interest here are the film formation and break-up processes that can be found in "air-blast" atomizers. One implementation of this atomization method consists of an array of plain orifices from which liquid jets impinge on an opposing filmer wall while being subjected to a crossflowing air stream [4,5]. The formation and spreading of a thin, uniform film are of considerable interest to fuel injector designers, as this determines both the spatial distribution of the fuel [4] and the primary droplet size [6] in the combustion device.

The concept of jet filming in the presence of a high-velocity crossflow is depicted in Fig. 1 to illustrate the various phenomena that are assumed to occur in the atomization process. Current computational and modeling techniques have limited capability to

resolve these processes for engineering-scale devices. There is also a strong need in this area for both diagnostic and model-validation data.

2 The Atomist Model

The approach used in this study is based on the time-dependent description of the liquid phase as well as on local atomization submodels that operate directly on the jet and film surfaces. Specifically, the Atomization Model Interfaced With Surface Tracking (AtoMIST), designed for the high-shear conditions found in certain injection devices of combustors or afterburners. In contrast to its predecessor the "blob model," where unrealistically large parcels of liquid fuel are released directly from the injection orifice [7–9], AtoMIST explicitly describes the evolution of the interface between the liquid and the gas phase. Because of this, the effects of gas shear flow on the liquid, the blockage effect of the liquid jet on the gas stream, the inertia of the jet column in responding to injection perturbations, and the combined effect of these factors on fuel spray transport are all captured to first order [10]. At the same time, the interface is sufficiently coarse to make the computational overhead added by the AtoMIST only a fraction of the typical cost of a full combustor simulation.

For many industrial applications, it is computationally prohibitive to describe the atomization process in terms of individual ligament pinching and droplet formation (but consider, for instance, Ref. [11]). The uniqueness of the proposed approach is to

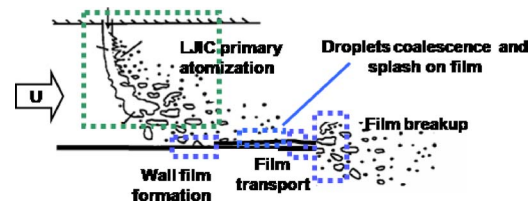


Fig. 1 Schematic of the major physics of fuel injection and filming in AtoMIST

¹Corresponding author.

Contributed by the International Gas Turbine Institute (IGTI) of ASME for publication in the JOURNAL OF ENGINEERING FOR GAS TURBINES AND POWER. Manuscript received April 17, 2010; final manuscript received April 25, 2010; published online November 10, 2010. Editor: Dilip R. Ballal.

explicitly calculate only large-scale features (i.e., comparable to the orifice diameter) of the liquid surface and to inject drops following the prescriptions of “subgrid” atomization models. These models are active in different zones of the injector (see Fig. 1) and their outline is presented next.

It is assumed that a coarse representation of the interface is available to provide the liquid volume fraction. Immediately after drop formation, the AtoMIST uses traditional Lagrangian description of a parcel as a collection of same-diameter drops that move at a common velocity. Before atomization, the single-fluid approach is adopted to describe the continuous phase. Specifically, properties such as density and viscosity depend on the cell-averaged value of the liquid volume fraction $0 \leq \alpha \leq 1$. The zero value of α (in fact, any value below a finite but small threshold) corresponds to the gas phase.

The main simplification of AtoMIST consists in transforming liquid elements of the jet or film surface into Lagrangian parcels (by atomization) and vice versa (by impingement) directly at the tracked liquid surface. This transformation is based on phenomenological or empirical prescriptions that depend on local flow characteristics. It is realized via mass and momentum transfers in the multiphase Navier–Stokes equations

$$\frac{\partial}{\partial t}(\alpha \rho_L) + \nabla \cdot (\alpha \rho_L \mathbf{v}) = S_\alpha \quad (1)$$

$$\frac{\partial}{\partial t}(\rho \mathbf{v}) + \nabla \cdot (\rho \mathbf{v} \mathbf{v}) = -\nabla p + \nabla \cdot [\mu(\nabla \mathbf{v} + \nabla \mathbf{v}^T)] + \mathbf{F}_\alpha \quad (2)$$

where $\rho = (1 - \alpha)\rho_G + \alpha\rho_L$ and $\mu = (1 - \alpha)\mu_G + \alpha\mu_L$. For instance, if a drop impinges on a wall or on a pre-existing film, its mass m_p appears in the source term

$$S_\alpha = \frac{m_p}{V\Delta t} \quad (3)$$

The subscript p denotes parcel quantities, V is the volume of the computational cell where impingement occurs, and Δt is the time step. Conversely, if a drop forms by atomization, a sink term is defined. The momentum that is lost or gained by the parcel becomes a force in the momentum equation

$$\mathbf{F}_\alpha = \frac{m_p \mathbf{v}_p}{V\Delta t} \quad (4)$$

This averaged force is distributed over the time period Δt . Thus, it is by adding source terms to the governing equations that the mass and momentum are conserved during the transformation from the dispersed to the continuous representation (or vice versa). A source term can similarly be added to the energy equation.

The formation of a drop or its impingement typically affects more than one cell. A search algorithm is in place to identify all the N_p closest cells until the target parcel mass m_p is reached

$$\sum_{j=1}^{N_p} \alpha_j V_j = \frac{m_p}{\rho_L} \quad (5)$$

In each of the neighboring N_p cells, the sink/source term is then set accordingly. In the case of drop formation, by running a sum over the tagged cells, the drop velocity is assigned as

$$\mathbf{v}_p = \frac{\sum_j \alpha_j V_j \mathbf{v}_j}{\sum_j \alpha_j V_j} \quad (6)$$

and the point of injection is the center of mass of the tagged cells weighted by volume fraction.

With reference to the configuration of Fig. 1, the process of film formation and breakup can be described in a sequence of steps starting from the fuel injection at the orifice.

1. Drops shed from the jet surface, and ligaments break up from the top of the liquid column (jet in crossflow primary atomization).
2. In equilibrating with the crossflow, drops and ligaments can undergo further fragmentation (secondary atomization).
3. During this process or afterwards, a fraction of the spray is transported by the crossflow to a liquid film patch on the filmer wall or to a dry portion of it.
4. The liquid in the film moves subject to shear from the gas phase.
5. Drops can be shed from the film surface; alternatively, impinging drops can remove liquid from the film by splashing.
6. The liquid reaches the end of the filmer wall, where the competition of surface tension and shear results in the formation of new ligaments and drops (film breakup).

Steps 2 and 4 concern a standard implementation of the discrete and continuous phase discretization and are described in the Sec. 4. Primary breakup in step 1 is original to this and previous work by the authors [12]. It results from the competition of three distinct submodels—turbulent primary breakup, surface stripping, and column breakup. Surface stripping also participates in step 5. Specific models for impingement and splashing (step 3) and for film breakup (step 6) are presented for the first time in this paper.

2.1 Shear Stripping. The stripping model is based on the analogy to the droplet secondary breakup in the shear breakup regime, where droplets are stripped at the periphery of the parent drop from the boundary layer that forms along the windward liquid surface. The diameter of the drop formed by pinching the boundary layer is

$$d_p = C_\delta \sqrt{\nu_L t_\delta} \quad (7)$$

where t_δ is the time a surface liquid element is exposed to shear, ν_L is the kinematic viscosity of the liquid, and C_δ is a model constant. The time t_δ needs to be tracked and updated for all computational cells on the liquid surface. Based on laminar boundary layer theory, $C_\delta = 3.36$. The assumptions that drop sizes after breakup are comparable to the thickness of the liquid boundary layer, and that the boundary layer in the liquid phase is laminar, can be traced to the description of aerodynamic effects on secondary breakup by Wu et al. [13].

We introduce the condition that allows the liquid boundary layer to be stripped off in the form

$$\rho_G \|U_G - U_L\|^2 \kappa > C_\sigma \frac{\sigma}{d_p^2} \quad (8)$$

The vectors U_G and U_L need to be averaged over the neighbors of the insertion cell in the gas and liquid phase, respectively. Equation (8) compares the “suction” exerted at the interface over an average surface curvature κ , on the right-end side of the equation, to the force per unit area that is needed to create a drop of diameter d_p . The constant C_σ accounts for the nonideality of this process and is set to 2.0. Curvature is calculated from the gradient of the liquid volume fraction of the neighboring cells

$$\kappa = \nabla \cdot \frac{\nabla \alpha}{|\nabla \alpha|} \quad (9)$$

As in all the following models, the parcel diameter and its mass are independent. In fact, the parcel mass can be interpreted as a flux over a surface area for a time step. In the current implementation, we suggest

$$m_p = \left(\frac{\rho_G \|U_L - U_L\|^2 \kappa d_p^2}{C_\sigma \sigma} - 1 \right) \rho_L \|U_G - U_L\| \frac{\pi d_p^2}{4} \Delta t \quad (10)$$

2.2 Turbulent Primary Breakup. This model assumes the occurrence of random jetting from the unsteady column surface. This description is based on experimental observations of a fully

turbulent liquid jet in the gas Weber number range from 0 to 280 [14], which suggest the prevalence of ligament tip breakup with drop-to-ligament diameter ratio close to 1.9—the value expected from Rayleigh–Plateau instability [15].

The onset of breakup occurs in a configuration where a surface turbulent eddy of characteristic size ℓ_i is jetting out at velocity v_{ℓ_i} ; the ligament then grows to the breakup length in the Rayleigh breakup time t_R . In the AtoMIST implementation, every surface fluid element is attributed a finite probability that the surface element will start jetting at a time t_{Ri} . Thus, by taking $d_p \sim \ell_i$ and $t_R \sim t - t_{Ri}$, the parcel diameter for the element at a later time t is estimated as

$$d_p = \left(\frac{\sigma}{\rho_L} \frac{t^2}{\ell_i} \right)^{1/3} \quad (11)$$

The parcel forms under the condition that the kinetic energy of the ligament is greater than the surface energy required to form a drop

$$\rho_L v_{\ell_i}^2 > C_\sigma \frac{\sigma}{\ell_i} \quad (12)$$

The eddy size ℓ_i is assumed to fall within the inertial range so that

$$v_{\ell_i} \sim v' (\ell_i / \Lambda)^{1/3} \quad (13)$$

where Λ is the cross-stream integral length scale of the flow at the orifice. According to the flow measurements of a fully developed turbulent pipe, $\Lambda \sim d_0/8$. The fluctuation v' can be estimated from an assumed turbulence intensity I_L and the local velocity. If condition Eq. (12) is satisfied, then the parcel diameter is

$$d_p = C_t \left(\frac{\sigma t^2}{\rho_{\text{liq}}} \right)^{1/3} \quad (14)$$

with mass

$$m_p = \left(\frac{C_t \rho_L I_L U_L^2 d_p}{C_\sigma \sigma} - 1 \right) \rho_L \|U_G - U_L\| \frac{\pi d_p^2}{4} \Delta t \quad (15)$$

In the current implementation, the turbulence intensity of the liquid phase is a constant (typically, $I_L = 0.03$) and C_t is set to 1.

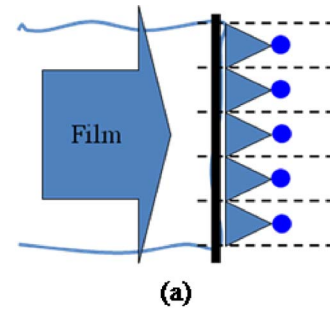
2.3 Column Breakup. This submodel predicts the instantaneous location of column breakup and creates one or more parcels whose size depends on the remaining mass of the liquid column downstream of the breakup point. This approach assumes that breakup is initiated by wave amplification of the Kelvin–Helmholtz type. The description of how the time to breakup of the column is estimated can be found in Ref. [9]. Recent analyses of the unsteady liquid jet in crossflow behavior are reported in Refs. [16,17].

2.4 Film Breakup. A simple model is adopted where the liquid film is atomized right after the film detaches from the filmer plate. The diameter is taken as proportional to the local thickness h .

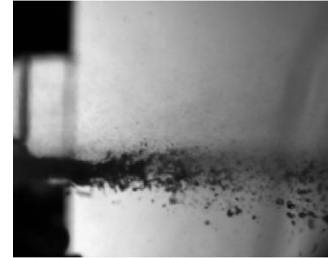
$$d_h = C_h h \quad (16)$$

This expression can be considered a limit case of prompt atomization [6] where the ratio by mass of atomizing air to liquid is very large. For the results presented here, $C_h = 6$. It is noted that additional effects, for instance, due to swirling flow, should be incorporated in a more complete film breakup prescription, which requires further study.

The thickness h is calculated directly over an area element A_h of the filmer wall by evaluating the liquid volume contained in the cylinder normal to it. In the calculations that will be shown next, the edge of the filmer wall is subdivided into six elements, each providing a local value of h , see Fig. 2. The calculated spray characteristics do not appear to be dependent on the specific number of subdivisions of the filmer edge. Similar to the injection process for jet atomization, the mass of the droplets formed by



(a)



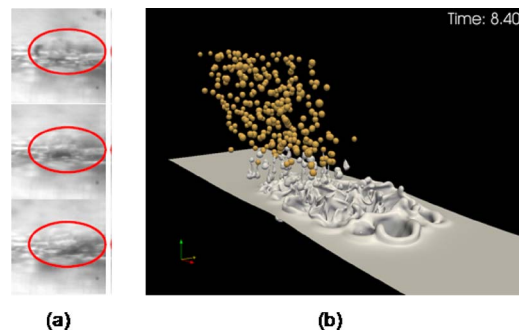
(b)

Fig. 2 (a) Film breakup model schematics (from the top of the film) and (b) snapshot of the film from the experiment (side view)

film breakup is found by collecting the amount of liquid volume fraction in neighboring cells, downstream of the edge element. Since this operation is currently carried out at every iteration, this mass depends on Δt times the element velocity. The velocity is calculated according to Eq. (6).

2.5 Splashing. The evolution of a thin liquid surface can be expected to be complicated when spray impingement distorts the already uneven film surface. In the frame sequence of Fig. 3(a) a liquid crown can be observed downstream of the impact of a drop on the film. The crown rapidly disintegrates into droplets that cannot be resolved by the optical system of the experiment (with $12 \mu\text{m}/\text{pixel}$ of resolution). A similar picture is shown in Fig. 3(b) from the simulation of drops with distribution between $20 \mu\text{m}$ and $50 \mu\text{m}$ impinging on a film of thickness $100 \mu\text{m}$. The calculation is carried out as a direct numerical simulation using the RLSG code [18].

The scenario above is sufficiently similar to the one described in the experiment by Samenfinck et al. [19], where droplets of $100 \mu\text{m}$ were injected in a 30 m/s airflow with incidence angle between 25 deg and 90 deg toward a $50\text{--}120 \mu\text{m}$ film. AtoMIST's splashing model is based on Samenfinck's empirical correla-



(a)

(b)

Fig. 3 (a) Snapshots ($15 \mu\text{s}$ apart) of drop impingement and (b) detailed numerical simulation

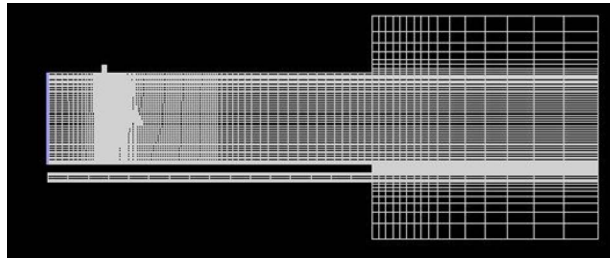


Fig. 7 Midplane cut of the computational grid

pressure-based solver using the implicit body force treatment to account for the surface tension term. Viscosity is augmented according to the Smagorinsky–Lilly model for eddy-viscosity [26] to include the effect of turbulence in the liquid and gas phase.

The computational grid is a stretched hexahedral mesh of 0.74×10^6 elements; see Fig. 7 for a cross section along the midplane. The grid stretches in orthogonal directions from the injection region. Two layers of refinement (with hanging nodes) based on the liquid volume fraction are also added to sufficiently resolve the liquid interface while keeping the grid count low. The choice of grid density is guided by a previous grid convergence study carried out by the authors [10,27]. According to that result, capturing bulk interface features of the jet requires at least ten computational elements per orifice diameter, corresponding to a grid spacing of the order of $100 \mu\text{m}$. A stretched, boundary layer grid is set at the filmer wall to accommodate the very thin film.

The grid extends spanwise by 15.24 mm, with symmetry boundary conditions on the sides. A gas inlet velocity inflow is assigned 6.34 mm upstream of the orifice, with pressure outflow at 55.37 mm downstream. A second velocity inflow condition is assigned at the liquid inlet. The crossflow is assumed to be fully turbulent, with a velocity profile $u_{\infty}(d_w/\delta_T)^{1/7}$ for $d_w < \delta_T$, where d_w is the distance from the test section walls and δ_T the turbulent boundary layer thickness at the inlet. For $d_w \geq \delta_T$, the velocity profile is uniform. The thickness δ_T is estimated following the relation for a fully developed boundary layer on a plate. The prescribed turbulence intensity and turbulent length scale are 3% and 2.54 mm at the crossflow inlet and 3% and 0.032 mm at the jet inlet.

4.2 Dispersed Phase Description. Droplet trajectories are calculated by the parcel approach, with each parcel representing several physical droplets with the same diameter and velocity. Once a parcel is injected in the flow field, its trajectory is calculated in Lagrangian form and updated at each time step of the unsteady flow calculation. Assuming spherical drops of diameter d_p , the drag coefficient is $C_d=0.424$ for $\text{Re}_p=\rho_L u_{rel} d_p/\mu_G > 1000$ and

$$C_d = \frac{24}{\text{Re}_p} \left(1 + \frac{1}{6} \text{Re}_p^{2/3} \right) \quad (18)$$

otherwise [28]. The droplet Reynolds number depends on the properties of the gas phase and on the relative velocity between drop and gas u_{rel} . Momentum coupling from the discrete to the continuous phase is included.

Droplets secondary breakup in the moderate Weber number regime of interest is modeled by the Taylor analogy breakup [29]. Each droplet trajectory is integrated with an additional stochastic velocity component that mimics turbulent fluctuations in the gas phase, following the standard discrete random walk approach [30]. The fluctuating velocity components are kept constant over a time interval τ , which depends on the turbulent eddies characteristic lifetime.

J = 52
We_g = 157
Crossflow Velocity: 74 m/s

J = 42
We_g = 193
Crossflow Velocity: 82 m/s

J = 34
We_g = 238
Crossflow Velocity: 91 m/s

J = 28
We_g = 287
Crossflow Velocity: 100 m/s

J = 24
We_g = 335
Crossflow Velocity: 108 m/s

J = 19
We_g = 157
Crossflow Velocity: 74 m/s

J = 15
We_g = 193
Crossflow Velocity: 82 m/s

J = 12
We_g = 238
Crossflow Velocity: 91 m/s

J = 10
We_g = 287
Crossflow Velocity: 100 m/s

J = 8.8
We_g = 335
Crossflow Velocity: 108 m/s

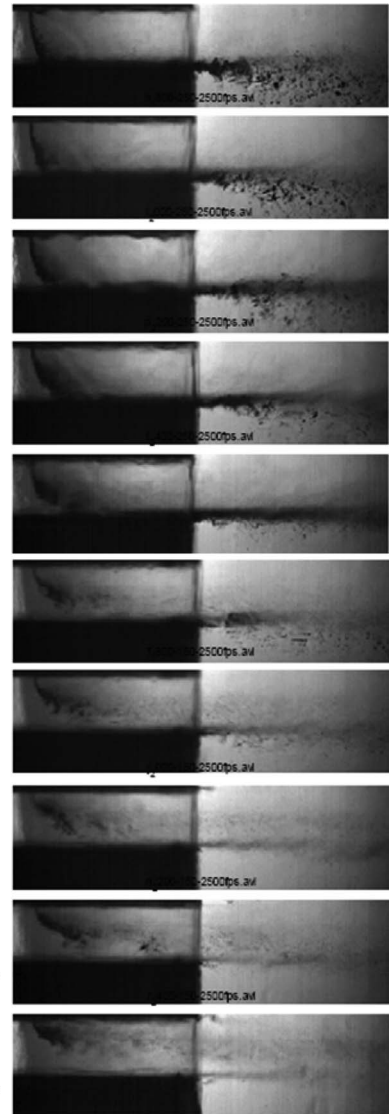


Fig. 8 Injection conditions and experiment side view

5 Results

The range of injection conditions of the experiments is shown in Fig. 8. The snapshots there demonstrate the role of jet penetration in forming the film as well as the effect of the filming surface on the atomization process. The volumetric flow of the droplets emerging from the film increases with the amount of liquid directly impinging on the surface, and, even at the lowest momentum-flux ratios, a significant stream of fine droplets is generated from the filming surface. Particularly, as the momentum-flux ratio increases to values of 20 and higher, a second distribution of droplets appears from the filming surface due to the liquid film flowing off the surface and breaking up.

From Fig. 8, two modes of droplet generation can be identified: a fine mist formed by film surface atomization before the liquid reached the edge of the plate; and larger spray drops due to the breakup of the film sheet at the filmer lip. Two simulation results are described here to show that AtoMIST captures the correct trend with increasing jet velocity at the same crossflow velocity of 82 m/s: case 1, with and $v_{jet}=12.7 \text{ m/s}$ ($J=15$, $We_G=193$) and case 2 with $v_{jet}=17 \text{ m/s}$ ($J=42$, $We_G=193$).

Before comparing the simulation results with the experiments, it is worth examining the appearance of the AtoMIST simulation in Fig. 9. In the snapshot, the jet and the film captured by the VOF

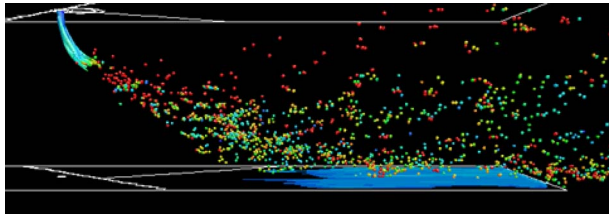


Fig. 9 Simulation snapshot. Parcels are colored by size from 0 μm to 100 μm . The $\alpha=0.5$ liquid fraction isosurface is colored by axial velocity from 0 m/s to 50 m/s.

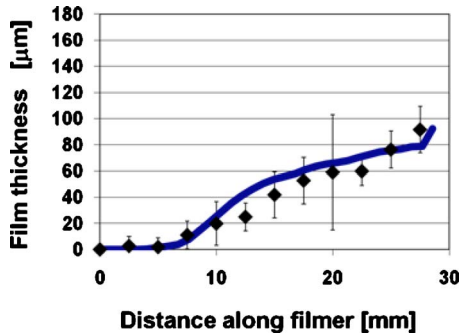


Fig. 10 Case 1 ($v_{\text{jet}}=12.7$ m/s): film thickness along the centerline. The 0 abscissa corresponds to the location of the orifice in the upper wall.

are shown as $\alpha=0.5$ isosurfaces colored by axial liquid velocity. Superimposed are the parcels, represented as equal-size sphere and colored by the value of their diameter. The smoothness of the liquid surface and the sharp transition to spherical drops emphasize the approximations that are built into AtomIST. In this example, most of the jet atomization occurs via column breakup, and a significant fraction of the newly formed ligaments undergoes secondary breakup. The smallest drops equilibrate with the crossflow before hitting the filmer plate and produce the fine mist leaving the test section. The remaining drops impinge on the wall and form a thin film of few tens of microns. A second stream of parcels develops from the filmer edge and exhibits a characteristic size that is essentially independent from the size imposed by the jet atomization.

The film thickness along the test section midplane are shown for the two injection velocities in Figs. 10 and 11. In the plots, the film thickness increases steadily and reaches a measured thickness of 90 μm and 140 μm for case 1 and case 2, respectively. The film is approximately 15 μm thicker in case 2 than in case 1. This is due to the increased mass flow rate through the injection orifice and to the related increased jet penetration, allowing fewer drops

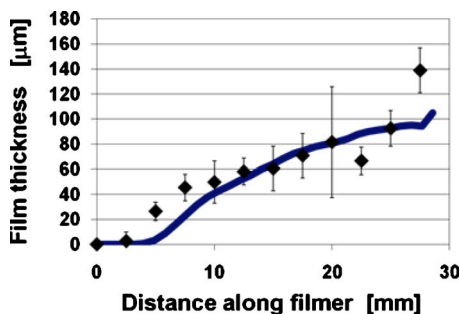


Fig. 11 Drop size and velocity in the transverse direction for case 1. The 0 ordinate corresponds to the location of the filmer wall.

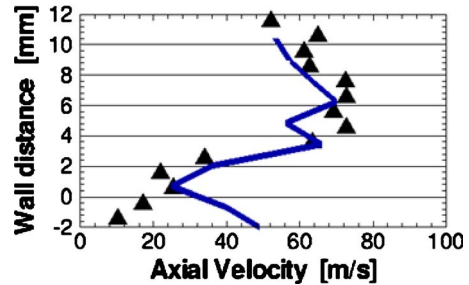
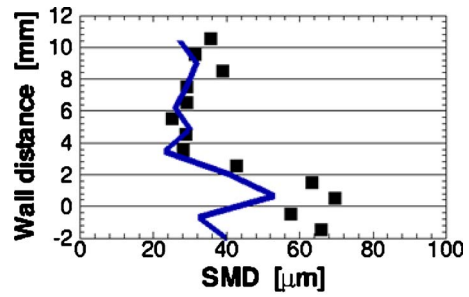


Fig. 12 Case 1 ($v_{\text{jet}}=17$ m/s): film thickness along the centerline. The 0 abscissa corresponds to the location of the orifice in the upper wall.

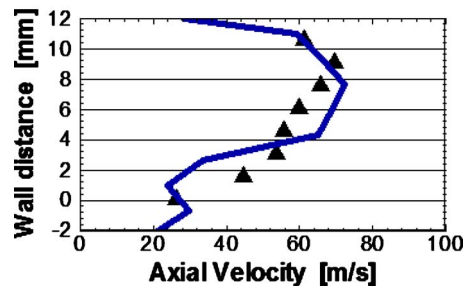
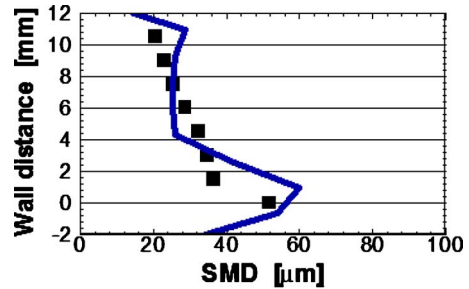


Fig. 13 Drop size and velocity in the transverse direction for case 2. The 0 ordinate corresponds to the location of the filmer wall.

to escape the impact with the wall for the same crossflow. The increased jet penetration can be detected by the earlier development of the film, which starts 6 mm downstream of the orifice in case 2 (Fig. 11) compared with 8 mm in case 1 (Fig. 10).

The velocity and Sauter mean diameter distribution from the PDDA measurements along the midplane and from the simulation results show the same trend in Figs. 12 and 13: increasing velocity and decreasing size with the distance from the filmer. Also, the largest droplet flux is observed just below the filmer plate, where the remainder of the liquid contained in the film is shed from the plate in large ligaments as opposed to small particles.

6 Conclusions

A new methodology for time-accurate, physics-based spray generation that can be coupled to unsteady combustor simulations is presented in this paper. By capturing the bulk response of the liquid column as well as the unsteady trajectory of the spray droplets, this technology enables affordable calculations that are less dependent on calibration than CFD state-of-the-art industrial spray models. The new approach for liquid film formation and breakup is a significant progress with respect to standard models based on a constant restitution coefficient for all the impinging parcels. This is shown by the good match with spray measurements from the filming experiment described here. Conceptual challenges still exist in providing a firm basis to the atomization models proposed here. Experimental observation and direct numerical simulation are currently being used for further refinement of AtOMIST.

Acknowledgment

The support of United Technologies, Corp., is gratefully acknowledged.

Nomenclature

C_d	= drop drag coefficient
C_h	= proportionality coefficient in prompt atomization model (default is 6)
C_t	= drop size coefficient in turbulent breakup model (default is 1)
C_δ	= liquid boundary layer thickness coefficient (default is 3.36)
C_σ	= drop formation condition coefficient (default is 2)
d_0	= jet orifice diameter
d_i	= impinging droplet diameter
d_p	= droplet diameter
d_w	= distance from test section walls
F_α	= source term in mass equation due to drop breakup/impingement
h	= local film thickness
H	= film thickness normalized by impinging droplets
I_L	= turbulence intensity of the liquid
J	= liquid to air flux momentum ratio
ℓ_i	= characteristic size of surface turbulent eddy
La	= Laplace number $La = \rho_L \sigma d_i / \mu_L^2$
Re_G	= droplet Reynolds number $Re_G = \rho_L u_{rel} d_p / \mu_G$
S_α	= source term in mass equation due to drop breakup/impingement
s_{cd}	= splashing momentum parameter
U	= mass-averaged velocity over cells neighboring the injection point
u_∞	= crossflow inlet velocity
u_{jet}	= inlet jet velocity
We_G	= crossflow Weber number $We_G = \rho_G u_\infty^2 d_0 / \sigma$
α	= liquid volume fraction
α_i and α_p	= incoming and outgoing trajectory angles
δ_T	= inlet turbulent boundary layer thickness
Λ	= turbulent integral scale
κ	= liquid surface curvature
μ	= dynamic viscosity
ν	= kinematic viscosity
ρ	= density
σ	= surface tension
τ	= random walk characteristic time

Subscripts

G = gas

L = liquid

p = particle

References

- [1] Mathews, W. S., Lee, C. F., and Peters, J. E., 2003, "Experimental Investigations of Spray/Wall Impingement," *Atomization Sprays*, **13**, pp. 223–242.
- [2] Panoa, M. R. O., and Moreira, A. L. N., 2005, "Experimental Characterization of an Intermittent Gasoline Spray Impinging Under Cross-Flow Conditions," *Atomization Sprays*, **15**, pp. 201–222.
- [3] Kiura, T., Shedd, T. A., and Blaser, B. C., 2009, "Investigation of Spray Evaporation and Numerical Model Applied for Fuel-Injection Small Engines," *SAE Int. J. Engines*, **1**, pp. 1402–1409.
- [4] Cohen, J. M., and Rosfjord, T. J., 1993, "Influences on the Sprays Formed by High-Shear Fuel Nozzle/Swirlers Assemblies," *J. Propul. Power*, **9**(1), pp. 16–27.
- [5] Becker, J., and Hassa, C., 2000, "Plain Jet Kerosene Injection Into High Temperature, High Pressure Crossflow With and Without Filmer Plate," Eighth International Conference on Liquid Atomization and Spray Systems, Pasadena, CA.
- [6] Lefebvre, A. H., 1989, *Atomization and Sprays*, Hemisphere Publishing Corp., New York.
- [7] Rachner, M., Becker, J., Hassa, C., and Doerr, T., 2002, "Modeling of the Atomization of a Plain Liquid Jet in Crossflow at Gas Turbine Conditions," *Aerosp. Sci. Technol.*, **6**, pp. 495–506.
- [8] Khosla, S., and Crocker, D. S., 2004, "CFD Modeling of the Atomization of Plain Liquid Jets in Cross Flow for Gas Turbine Applications," ASME Paper No. GT2004-54269.
- [9] Madabhushi, R. K., Leong, M. Y., and Hautman, D. J., 2004, "Simulation of the Breakup of a Liquid Jet in Crossflow at Atmospheric Conditions," ASME Paper No. GT2004-54093.
- [10] Arienti, M., Madabhushi, R. K., van Slooten, P. R., and Soteriou, M. C., 2006, "Aerodynamic Blockage Effect on the Spray Characteristics of a Liquid Jet Atomized by Crossflowing Air," ASME Paper No. GT2006-90536.
- [11] Li, X., Arienti, M., Soteriou, M. C., and Sussman, M., 2010, "Towards an Efficient, High-Fidelity Methodology for Liquid Jet Atomization Computations," Forty-Eighth AIAA Aerospace Sciences Meeting, Paper No. AIAA-2010-0210.
- [12] Arienti, M., and Soteriou, M. C., 2007, "Dynamics of Pulsed Jet in Crossflow," ASME Paper No. GT2007-27816.
- [13] Wu, P.-K., Hsiang, L.-P., and Faeth, G. M., 1995, "Aerodynamic Effects on Primary and Secondary Spray Breakup," *Liquid Rocket Engine Combustion Instability Progress in Aeronautics and Astronautics*, **169**, pp. 247–279.
- [14] Wu, P.-K., Tseng, L.-K., and Faeth, G. M., 1992, "Primary Breakup in Gas/Mixing Layers for Turbulent Liquids," *Atomization Sprays*, **2**, pp. 295–317.
- [15] Aalburg, C., Faeth, G. M., and Sallam, K. A., 2005, "Primary Breakup of Round Turbulent Liquid Jets in Uniform Gaseous Crossflows," AIAA Paper No. 2005-0734.
- [16] Arienti, M., and Soteriou, M. C., 2009, "Time-Resolved Proper Orthogonal Decomposition of Liquid Jet Dynamics," *Phys. Fluids*, **21**, p. 112104.
- [17] Herrmann, M., Arienti, M., and Soteriou, M. C., 2010, "The Impact of Density Ratio on the Primary Atomization of a Turbulent Liquid Jet in Crossflow," ASME Paper No. GT2010-23016.
- [18] Herrmann, M., 2008, "A Balanced Force Refined Level Set Grid Method for Two-Phase Flows on Unstructured Flow Solver Grids," *J. Comput. Phys.*, **227**, pp. 2674–2706.
- [19] Samenfinck, W., Elsaber, A., Dullenkopf, K., and Wittig, S., 1999, "Droplet Interaction With Shear-Driven Liquid Films: Analysis of Deposition and Secondary Droplet Characteristics," *Int. J. Heat Fluid Flow*, **20**, pp. 462–469.
- [20] Shedd, T., Corn, M. L., Arienti, M., and Soteriou, M. C., 2009, "Liquid Jet Breakup by an Impinging Air Jet," Forty-Seventh AIAA Aerospace Sciences Meeting, Paper No. AIAA-2009-0998.
- [21] Wypych, G., 2000, "Knovel Solvents—A Properties Database," ChemTec Publishing, <http://www.knovel.com/knovel2/Toc.jsp?BookID=635&VerticalID>
- [22] Shedd, T. A., and Newell, T. A., 1998, "Automated Optical Liquid Film Thickness Measurement Method," *Rev. Sci. Instrum.*, **69**(12), pp. 4205–4213.
- [23] Rodriguez, D. J., 2004, "Characterization of Bubble Entrainment, Interfacial Roughness and the Sliding Bubble Mechanism in Horizontal Annular Flow," Ph.D. thesis, University of Wisconsin-Madison.
- [24] <http://www.fluent.com/software/fluent/index.htm>
- [25] Ubbink, O., and Issa, R. I., 1999, "A Method For Capturing Sharp Fluid Interface on Arbitrary Meshes," *J. Comput. Phys.*, **153**, pp. 26–50.
- [26] Smagorinsky, J., 1963, "General Circulation Experiments With the Primitive Equations. I. The Basic Experiment," *Mon. Weather Rev.*, **91**, pp. 99–164.
- [27] Arienti, M., Madabhushi, R. K., Van Slooten, P. R., and Soteriou, M. C., 2005, "Numerical Simulation of Liquid Jet Characteristics in a Gaseous Crossflow," Proceedings of ILASS Americas.
- [28] Liu, A. B., Mather, D., and Reitz, R. D., 1993, "Modeling the Effects of Drop Drag and Breakup on Fuel Sprays," SAE Technical Paper No. 930072.
- [29] O'Rourke, P. J., and Amsden, A. A., 1987, "The TAB Method for Numerical Calculation of Spray Droplet Breakup," SAE Technical Paper No. 872089.
- [30] Gosman, A. D., and Ioannides, E., 1983, "Aspects of Computer Simulation of Liquid-Fueled Combustors," *J. Energy*, **7**, pp. 482–490.